



Article

Assembly of Homochiral Magneto-Optical Dy₆ Triangular Clusters by Fixing Carbon Dioxide in the Air

Cai-Ming Liu ^{1,2,*} , Xiang Hao ¹ and Xi-Li Li ³ 

¹ Beijing National Laboratory for Molecular Sciences, CAS Key Laboratory of Organic Solids, Institute of Chemistry, Chinese Academy of Sciences, Beijing 100190, China; haoxiang@iccas.ac.cn

² School of Chemical Sciences, University of Chinese Academy of Sciences, Beijing 100049, China

³ Henan Provincial Key Laboratory of Surface and Interface Science, Zhengzhou University of Light Industry, Zhengzhou 450002, China; lixl@zzuli.edu.cn

* Correspondence: cmliu@iccas.ac.cn

Abstract: A new hydrazone Schiff base bridging ligand (H₂L_{Schiff} (*E*)-*N'*-((1-hydroxynaphthalen-2-yl)methylene)pyrazine-2-carbohydrazide) and *L/D*-proline were used to construct a pair of homochiral Dy₆ cluster complexes, [Dy₆(CO₃)(*L*-Pro)₆(L_{Schiff})₄(HL_{Schiff})₂]·5DMA·2H₂O (*L*-1, *L*-HPro = *L*-proline; DMA = *N,N*-dimethylacetamide) and [Dy₆(CO₃)(*D*-Pro)₆(L_{Schiff})₄(HL_{Schiff})₂]·5DMA·2H₂O (*D*-1, *D*-HPro = *D*-proline), which show a novel triangular Dy₆ topology. Notably, the fixation of CO₂ in the air formed a carbonato central bridge, playing a key role in assembling *L*-1/*D*-1. Magnetic measurements revealed that *L*-1/*D*-1 displays intramolecular ferromagnetic coupling and magnetic relaxation behaviours. Furthermore, *L*-1/*D*-1 shows a distinct magneto-optical Faraday effect and has a second harmonic generation (SHG) response (1.0 × KDP) at room temperature. The results show that the immobilization of CO₂ provides a novel pathway for homochiral multifunctional 4f cluster complexes.

Keywords: chiral complexes; Dy(III) cluster complexes; fixation of carbon dioxide; magneto-optical Faraday effect; SHG response



Citation: Liu, C.-M.; Hao, X.; Li, X.-L. Assembly of Homochiral Magneto-Optical Dy₆ Triangular Clusters by Fixing Carbon Dioxide in the Air. *Molecules* **2024**, *29*, 3402. <https://doi.org/10.3390/molecules29143402>

Academic Editors: Andrea Bencini and Vito Lippolis

Received: 25 June 2024

Revised: 15 July 2024

Accepted: 18 July 2024

Published: 19 July 2024



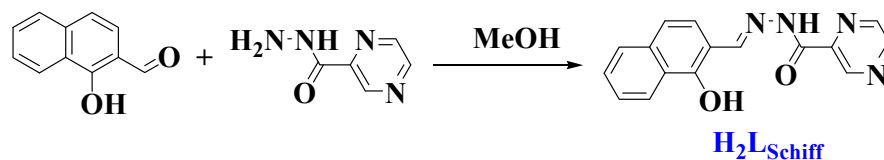
Copyright: © 2024 by the authors. Licensee MDPI, Basel, Switzerland. This article is an open access article distributed under the terms and conditions of the Creative Commons Attribution (CC BY) license (<https://creativecommons.org/licenses/by/4.0/>).

1. Introduction

While carbon dioxide emissions are contributing to increasing global warming, nature's carbon cycle tells us that fixing carbon dioxide in the air into organic compounds and molecular materials is the best solution. Especially, the fixation of carbon dioxide in the air as a structural component (such as carbonato) of functional complexes is a simple but effective method because it can be carried out automatically during the synthesis process [1]. More importantly, such functional complexes formed by the immobilization of CO₂ are usually not available directly with carbonate salts, or their structures are different from those of the products when carbonate salts are used directly [2]. So far, there have been some reports of 4f [3–13], 3d [14–19], and 3d–4f complexes [20–29] containing the carbonato bridge formed by the fixation of CO₂. Notably, the automatic fixation of CO₂ can play a critical structurally oriented role in the construction of single-molecule magnets (SMMs) [2,4–13,20–29]. The SMMs are nanoscale molecules that exhibit magnetic bistability at blocking temperatures and are expected to be used in high-density information storage, molecular electronics, and quantum computing [30–38]. However, the SMMs involved in the fixation of CO₂ are still limited to achiral complexes [2,4–13,20–29].

Recently, we have been working on the construction of homochiral 3d–4f [39] and 4f [40–42] SMMs with Schiff base ligands to obtain strong magneto-optical Faraday effects, and such molecular materials have potential applications in magnetic-optical isolators, magnetic-optical switches, and other fields [43–46]. Furthermore, chiral SMM-induced magnetochiral dichroism (MChD) is expected to be used in the optical readout of magnetic storage data [47]. Generally, homochiral Schiff base ligands [39] and homochiral

β -diketone ligands [40–42] are selected to construct such homochiral SMMs, as these two types of ligands have characteristic Cotton peaks in the circular dichroism (CD) spectra, which facilitates the study of magneto-optical Faraday effects using magnetic circular dichroism (MCD) spectra. We hope that this research will be extended to the construction of magneto-optical SMMs with simpler and cheaper chiral carboxylic acid ligands. In this paper, we adopted *L/D*-proline as the homochiral ligand and a new hydrazone Schiff base ligand condensed with 1-hydroxy-2-naphthaldehyde and pyrazinoic acid hydrazide as the bridging ligand (H_2L_{Schiff} , Scheme 1) to assemble a pair of Dy_6 triangular cluster complexes, $[Dy_6(CO_3)(L-Pro)_6(L_{Schiff})_4(HL_{Schiff})_2] \cdot 5DMA \cdot 2H_2O$ ($L-1$, H_2L_{Schiff} (*E*)- N' -(1-hydroxynaphthalen-2-yl)methylene)pyrazine-2-carbohydrazide; $L-HPro$ = *L*-proline; DMA = *N,N*-dimethylacetamide) and $[Dy_6(CO_3)(D-Pro)_6(L_{Schiff})_4(HL_{Schiff})_2] \cdot 5DMA \cdot 2H_2O$ ($D-1$, $D-HPro$ = *D*-proline). $L-1/D-1$ is featured by the immobilization of CO_2 in the air during the assembly process; the corresponding carbonate ligand bridges three Dy^{3+} ions to form the central Dy_3 triangle, which is further linked to three outer Dy^{3+} ions via the $HL_{Schiff}^-/L_{Schiff}^{2-}$ and $L-Pro^-$ mixed bridges, generating a larger Dy_6 triangular cluster. Such a triangular Dy_6 topology has never been reported in carbonate-bridged Dy_6 cluster complexes. Notably, in addition to intramolecular ferromagnetic coupling and magnetic relaxation at 0 Oe, $L-1/D-1$ shows a magneto-optical Faraday effect and an SHG response at room temperature.



Scheme 1. Synthesis pathway of the new hydrazone Schiff base ligand H_2L_{Schiff} .

2. Results and Discussion

2.1. Synthesis and Crystal Structures

When the $Dy(III)$ complexes are assembled with hydrazone Schiff base ligands in an alkaline solution, the automatic fixation of CO_2 in the air can occasionally occur, and the carbonate-bridged $Dy(III)$ cluster complexes are finally obtained [2,4,6,8,12], which include Dy_6 complexes with topologies of the triangular prism [2,8,12] and the fusion of three capped triangular Dy_3 motifs [4]. $L-1/D-1$ was yielded by the reaction of 0.25 mmol of H_2L_{Schiff} , 0.25 mmol of $Dy(CF_3SO_3)_3$, 0.25 mmol of *L/D*-proline, and 0.75 mmol of $LiOH \cdot H_2O$ in 5 mL of DMA for 24 h at room temperature. In general, the reaction at room temperature can effectively prevent the rapid racemization of chiral complexes at high temperatures [48]. Good-quality single crystals of $L-1/D-1$ could be obtained by recrystallization with CH_2Cl_2 - $MeOH$ (1:1 *v/v*), which crystallizes in the monoclinic C_2 space group. If DMA is changed to DMF , the product with the same structure can also be obtained, but the lattice solvent DMA becomes DMF , and the single crystal diffraction data will be worse. Notably, the $Dy(III)$ cluster complexes constructed with *L/D*-proline are very rare [49], and $L-1/D-1$ represents the first complex constructed from the hydrazone Schiff base ligand H_2L_{Schiff} .

As shown in Figure 1a, the carbonate ligand formed by the automatic fixation of CO_2 in the air acts as the structural core of $L-1$, which directly bridges three Dy^{3+} ions in a triangular shape in a hexadentate μ_3 -mode, with $Dy \dots Dy$ separation distances of 4.793, 4.867, and 4.745 Å for Dy_2 - Dy_3 , Dy_3 - Dy_5 , and Dy_2 - Dy_5 , respectively. Such a CO_3^{2-} -bridged Dy_3 central triangle is further linked to three additional Dy^{3+} ions through the $HL_{Schiff}^-/L_{Schiff}^{2-}$ and $L-Pro^-$ mixed bridges, eventually forming a larger Dy_6 triangular cluster, which contains three small outer Dy_3 triangles. Such a triangular Dy_6 topology is different from the triangular prism [2,8,12] and the fusion of three capped triangular Dy_3 motifs [4] in carbonate-bridged Dy_6 cluster complexes. The outer $Dy \dots Dy$ separation distances are 3.987 Å for Dy_2 - Dy_4 , 3.930 Å for Dy_5 - Dy_4 , 3.959 Å for Dy_1 - Dy_2 , 3.906 Å for Dy_1 - Dy_3 , 3.926 Å for Dy_3 - Dy_6 , and 3.931 Å for Dy_5 - Dy_6 , which are smaller than those in

the Dy₃ central triangle (4.745–4.867 Å). Notably, the $\mu_3\text{-}\eta^2\text{:}\eta^2\text{:}\eta^2$ coordination mode of the carbonato ligand in *L-1* is also observed in the triangular prism-like Dy₆ cluster complexes assembled by other hydrazone Schiff base ligands [2,8,12] but is different from the $\mu_3\text{-}\eta^2\text{:}\eta^2$ coordination mode in the Dy₆ cluster complex with a topology of the fusion of three capped triangular Dy₃ motifs [4] and the $\mu_4\text{-}\eta^1\text{:}\eta^2\text{:}\eta^1\text{:}\eta^1$ coordination mode in the tub-like Dy₈ cluster complex [2,6]. The Schiff base ligands in *L-1* have not only a deprotonated form (L_{Schiff}^{2-}) but also a protonated form (HL_{Schiff}^-); both bridge the two Dy³⁺ ions on the outer Dy-Dy edge of the outer small Dy₃ triangle, and this Dy-Dy edge is simultaneously bridged by the carboxyl group of one *L-Pro*[−] anion; the latter adopts a unique $\mu_2\text{-}\eta^1\text{:}\eta^2$ coordination mode in which the pyrrolidine N atom does not participate in the coordination, while it usually uses both the carboxyl O atom and the pyrrolidine N atom to participate in coordination [49].

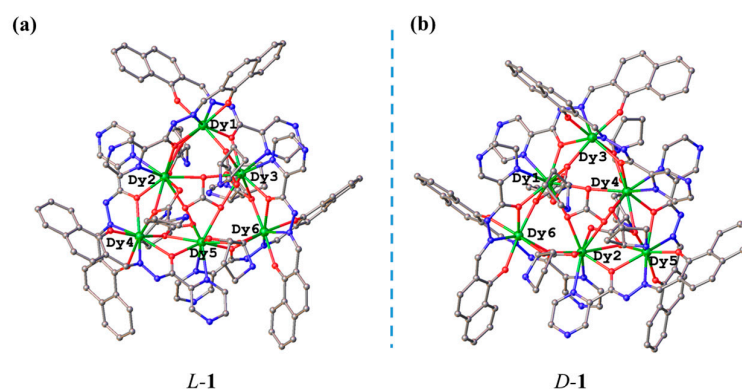


Figure 1. Crystal structures of *L-1* (a) and *D-1* (b). Color code: C, grey; N, blue; O, red; Dy, green. All disordered pyrrolidine rings show only one of two sets, and all H atoms and solvent molecules are omitted for clarity.

The Dy³⁺ ions located on the central Dy₃ triangle (Dy2, Dy3, and Dy5) are 10-coordinated (Figure 1), which are coordinated by two O atoms from the carbonato ligand, four O_{carboxyl} atoms from two *L-Pro*[−] anions, two O_{carboxyl} atoms and two N_{pyrazine} atoms from two $L_{\text{Schiff}}^{2-}/HL_{\text{Schiff}}^-$ ligands. An accurate analysis by the Shape 2.1 software [50] revealed that the coordination configurations of these Dy³⁺ ions are the bicapped square antiprism J17 (D_{4d}), and the CShM values are 2.886 for Dy2, 3.156 for Dy3, and 3.052 for Dy5 (Table S1). However, the Dy³⁺ ions located at the vertices of the large Dy₆ triangle (Dy1, Dy4, and Dy6) are 8-coordinated (Figure 1), which are bonded by two O_{carboxyl} atoms from two *L-Pro*[−] anions, two O_{carboxyl} atoms, two N_{pyrazine} atoms and two O_{phenol} atoms from two $L_{\text{Schiff}}^{2-}/HL_{\text{Schiff}}^-$ ligands. An accurate analysis by the Shape 2.1 software [50] showed that the coordination configurations of these three Dy³⁺ ions are the following: the biaugmented trigonal prism J50 (C_{2v}) for Dy1 and Dy4, with CShM values of 2.249 and 2.679, respectively (Table S2); the biaugmented trigonal prism (C_{2v}) for Dy6, with a CShM value of 2.118 (Table S2). *D-1* is an enantiomer of *L-1* and thus has a structure that is similar and mirror symmetrical to *L-1* (Figure 1b).

2.2. Magnetic Properties

The temperature-dependent DC magnetic susceptibility of *L-1* measured at 1000 Oe revealed that its $\chi_{\text{M}}T$ value ($85.10 \text{ cm}^3 \text{ K mol}^{-1}$) at 300 K is in agreement with the theoretical value of six isolated Dy³⁺ ions ($85.02 \text{ cm}^3 \text{ K mol}^{-1}$) (Figure 2). The $\chi_{\text{M}}T$ value of *L-1* decreases as it cools down, reaching a minimum of $65.44 \text{ cm}^3 \text{ K mol}^{-1}$ at 10 K, and then suddenly increases to $69.55 \text{ cm}^3 \text{ K mol}^{-1}$ at 2 K. Such a hook-like $\chi_{\text{M}}T$ -T curve is the result of a combination of two main factors: the depopulation of the m_j levels of the Dy³⁺ ions and the intramolecular ferromagnetic coupling among the Dy³⁺ ions [12,40,42,51]. Similar intramolecular ferromagnetic interactions between Dy³⁺ ions are also present in another carbonato-bridged dysprosium (III) complex [6]. Moreover, the magnetic field-dependent

magnetization measurements of *L-1* showed no overlap in the $M-H/T$ curves at 2–6 K (Figure S1), indicating magnetic anisotropy.

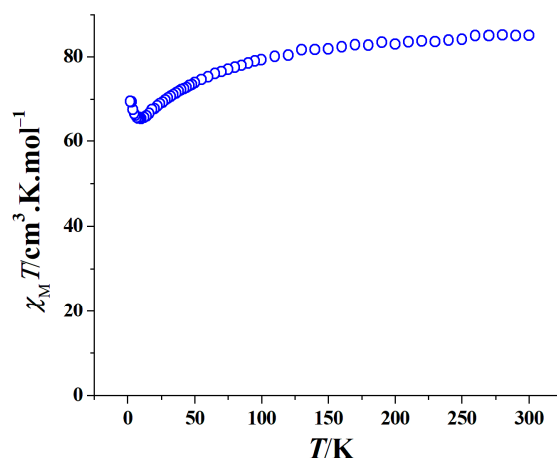


Figure 2. Plot of $\chi_M T$ vs. T of *L-1* ($H_{dc} = 1000$ Oe).

The temperature-dependent AC magnetic susceptibility of *L-1* was measured in the range of 50–1399 Hz at 0 Oe to investigate its SMM properties. The χ'' vs. T curves show frequency dependence, but no peaks, and the χ'' signal appears only in the lower temperature region (<5 K) (Figure 3), suggesting that the effective energy barrier value of *L-1* is very small. Furthermore, the $\chi''-T$ curve at 1399 Hz also shows no signs of peaking when a common DC field of 2000 Oe is applied (Figure S2), suggesting that the failure to show peaks is not caused by the quantum tunnelling effect. Such a phenomenon also occurs in the Dy_5 cluster complexes constructed from *L/D*-proline [49] and other $Dy(III)$ cluster complexes formed by the immobilized CO_2 [5,7].

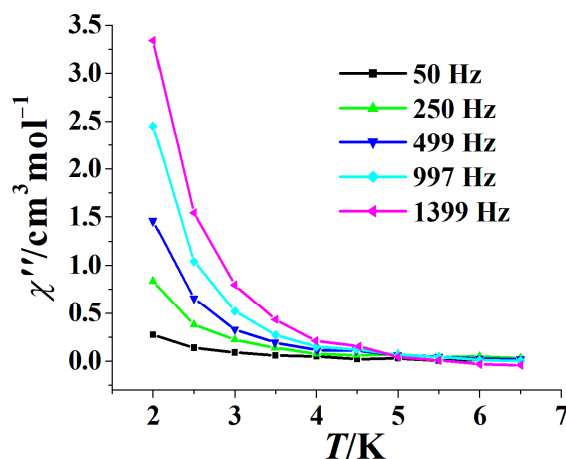


Figure 3. Plots of χ'' vs. T for *L-1* ($H_{dc} = 0$ Oe).

The Debye model based on Equation (1), in which $\omega (=2\pi\nu)$ represents the angular frequency [52], can generally be used to roughly estimate the U_{eff}/k value and the τ_0 value [53].

$$\ln(\chi''/\chi') = \ln(\omega\tau_0) + U_{eff}/kT \quad (1)$$

It is worth mentioning that such a fitting method is only suitable for when the $\chi''-T$ curves do not have peaks, and the U_{eff}/k and τ_0 values may be different when fitting with $\chi''-T$ curves of different frequencies [54]. The best fitting of $\ln(\chi''/\chi')-1/T$ curves for *L-1* leads to U_{eff}/k values of 6.5–8.3 K and τ_0 values of 2.0×10^{-7} – 6.5×10^{-7} s (Figure S3). The U_{eff}/k value of *L-1* is comparable with that of the hourglass-like $\{Dy_7\}$ cluster complex (~4.6 K) [53]. In Dy^{3+} multinuclear cluster complexes, the magnetic axes of different ions are

difficult to regularize, and factors such as J-type exchange coupling and intramolecular and intermolecular dipole interactions are often not conducive to good SMM performance [32]; these factors are also likely to be the reason for the smaller U_{eff}/k value of *L-1*.

2.3. Circular Dichroism Spectra (CD) and Magnetic Circular Dichroism Spectra (MCD)

In order to verify the properties of the enantiomers, the CD spectra of *L-1* and *D-1* in DMF solution were measured along with their UV-vis spectra (Figure 4). The UV-vis spectrum of *L-1* is similar to that of *D-1* (Figure 4, below), the strong peak at 322 nm may be ascribed to the π - π^* conjugation of the naphthalene ring and the C=N bond of the hydrazone Schiff base ligand, while the strong peak at 454 nm and its shoulder peak at a higher wavelength are attributed to the n - π^* transition of the C=N bond of the hydrazone Schiff base ligand [39,41,42,45,46]. In contrast, the UV-vis spectrum of the H_2L_{Schiff} ligand in DMF solution can clearly distinguish the absorption peaks of the pyrazine group (323 nm), 1-naphthol group (338 nm) [55], and the π - π^* conjugation of the naphthalene ring and the C=N bond (373 nm), while the absorption peak of the n - π^* transition of the C=N bond at 475 nm is very weak (Figure S4). The CD spectra of *L-1* and *D-1* exhibit excellent mirror symmetry, confirming their enantiomeric properties (Figure 4, above). The Cotton peak at 298 nm is assigned to the π - π^* transitions of the conjugated group in the hydrazone Schiff base ligand, while the Cotton peaks at 374 nm and 428 nm are caused by the π - π^* and n - π^* transitions of the C=N chromophore, respectively [42,45,46].

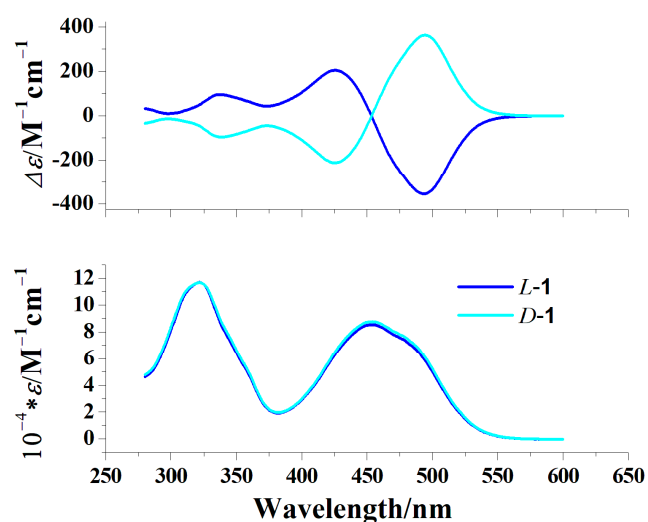


Figure 4. CD spectra of *L-1* and *D-1* in DMF solution ($c = 0.2 \text{ gL}^{-1}$; $H = 0 \text{ T}$) (above) and UV-vis spectra of *L-1* and *D-1* in DMF solution ($c = 0.2 \text{ gL}^{-1}$; $H = 0 \text{ T}$) (below).

To study the magneto-optical properties of *L-1* and *D-1*, we further measured their CD spectra when a magnetic field ($\pm 1.6 \text{ T}$) was applied (Figure 5). It should be noted that the positive (+1.6 T, NS) and negative magnetic fields (-1.6 T , SN) refer to the parallel and antiparallel direction of the magnetic field to the polarized light, respectively. As shown in Figure 5, the CD spectra of *L-1* and *D-1* under the $\pm 1.6 \text{ T}$ magnetic field also have mirror symmetry: the *D-1* (NS, +1.6 T) curve is mirror symmetrical with *L-1* (SN, -1.6 T), while the *D-1* (SN, -1.6 T) curve is mirror symmetrical with *L-1* (NS, +1.6 T). Notably, the positions of the Cotton peaks of the CD spectra of *L-1* and *D-1* at $\pm 1.6 \text{ T}$ are similar to those of their CD spectra at 0 T. The pure MCD signals *L-1* and *D-1* could be obtained based on $\text{MCD} = [\text{CD}(\text{NS}) - \text{CD}(\text{SN})]/2/M$ (here $M = 1.6 \text{ T}$) [38,40,41,44,45]. The pure MCD spectra show strong troughs at 350 nm and 437 nm for *L-1* and at 350 nm and 437 nm for *D-1* (Figure S5); these two troughs for each isomer are ascribed to the π - π^* and n - π^* transitions of the C=N chromophore, respectively [42,45,46].

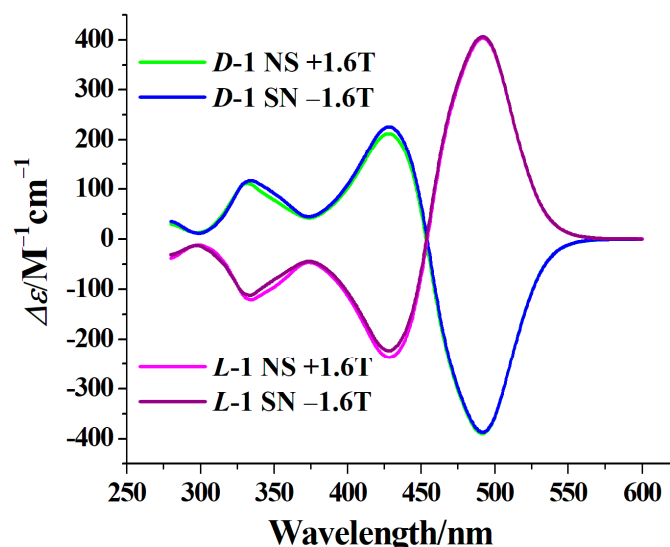


Figure 5. CD spectra of *L-1* and *D-1* in DMF solution under an NS (+1.6 T) or SN (−1.6 T) field ($c = 0.2 \text{ gL}^{-1}$; optical path = 5 mm).

The g_{MCD} values of *L-1* and *D-1* were then calculated based on $g_{\text{MCD}} = 2(\epsilon_+(B) - \epsilon_+(-B))/(\epsilon_+(B) + \epsilon_+(-B))$ [56] because the $|g_{\text{max(MCD)}}|$ value can be used to estimate the strength of the magneto-optical Faraday effect [56]. As shown in Figure S6, the $|g_{\text{max(MCD)}}|$ values of *L-1* and *D-1* at room temperature are 0.026 T^{-1} and 0.027 T^{-1} , respectively; these values are comparable with those of the homochiral 3d–4f complexes [R,R-/S,S-ZnLDy(H₂O)(NO₃)₃] {H₂L = 2-((E)-((1R,2R)/(1S,2S)-2-((E)-2-hydroxy-3-methoxybenzylideneamino)-1,2-diphenylethylimino)methyl)-6-methoxyphenol} (0.067 T^{-1}) [46] and [Mn₁₀Ln₆(R-/S-L₁)₆(L₂)₂(Ac)₁₂(μ₅-O)(μ₄-O)₆(μ₃-OH)₆(μ₂-H₂O)₂][Mn₆Ln₂(R-/S-L₁)₆(L₂)₂(Ac)₂(μ₄-O)₂(μ₃-OH)₂(H₂O)₂]-4ClO₄·10H₂O·CH₃CH₂OH {R-/S-H₂L = (R)-/(S)-2-(((1-hydroxybutan-2-yl)imino)methyl)-5-methoxyphenol; HL₂ = 2-hydroxy-4-methoxybenzaldehyde} (0.012 T^{-1}) [44], but are obviously smaller than those of 4f SMMs based on homochiral β-diketone ligands ($\geq 0.34 \text{ T}^{-1}$) [40–42] and Cu-Dy zero-field SMMs ($\geq 0.44 \text{ T}^{-1}$) [39,45]. This may be related to the fact that the SMM properties of *L-1* and *D-1* are not as good as the latter.

2.4. Nonlinear Optical Properties

Since *L-1/D-1* is a chiral crystalline complex, we investigated its second-order nonlinear optical properties. The second harmonic generation (SHG) efficiency of *L-1* is as strong as that of the reference sample KDP (KH₂PO₄) (Figure 6), and the SHG intensity of *L-1* ($1.0 \times \text{KDP}$) is equal to that of [DyZn₂(S,S-L_{Schiff})Cl₂(H₂O)][DyZn₂(S,S-L_{Schiff})Cl₂(MeOH)](ClO₄)₂·MeOH·0.5H₂O ($1.0 \times \text{KDP}$) and [DyZn₂(S,S-L_{Schiff})Br₂(H₂O)][DyZn₂(S,S-L_{Schiff})Br₂(MeOH)](CF₃SO₃)₂ ($1.0 \times \text{KDP}$) [57], but is obviously larger than those of chiral Dy(III) SMMs ($0.7 \times \text{KDP}$) [58] and other chiral Zn-Ln SMMs ($\leq 0.2 \times \text{KDP}$) [26,59,60]. Therefore, *L-1/D-1* is a potential second-order nonlinear optical molecular material. By the way, simultaneous measurements showed that *L-1/D-1* does not show any third-order nonlinear optical properties, which may be due to the lack of a strong electronic push–pull group in the ligand of *L-1*.

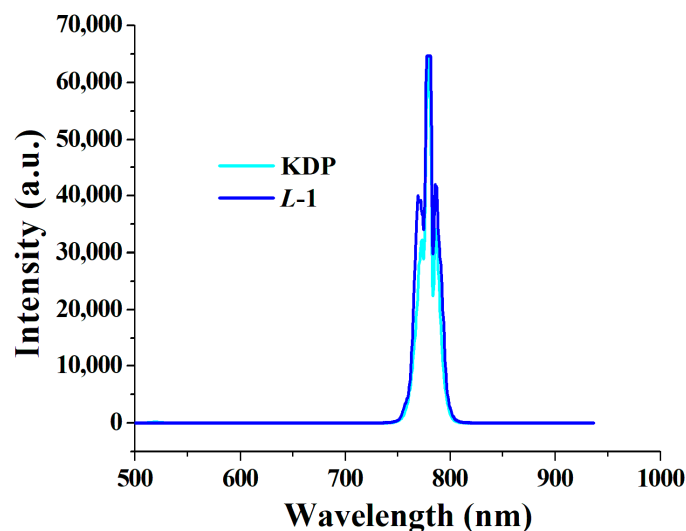


Figure 6. SHG spectra of crystalline samples of *L-1* and KDP under excitation at $\lambda = 1550$ nm ($T_{\text{int}} = 0.5$ s).

3. Experimental Section

All chemicals were analytically pure, purchased from commercial suppliers, and ready for use.

3.1. Materials and Instruments

The elemental analyses (C, H, N) were determined using a Thermo Flash Smart (Thermo Fisher Scientific, Waltham, MA, USA) elemental analyzer. The infrared spectra were recorded on a Bruker VERTEX 70v spectrophotometer (BRUKER OPTICS, Karlsruhe, Germany) using pressed KBr pellets. The UV-vis spectrum of $\text{H}_2\text{L}_{\text{Schiff}}$ was measured on a UH5700 Spectrophotometer (Hitachi hi-tech Co., Ltd., Tokyo, Japan). The circular dichroism (CD) spectra were recorded on a JASCO J-1700 spectropolarimeter (JASCO, Tsukuba, Japan) at room temperature with a 5 mm optical path, and a permanent magnet (+1.6 or -1.6 T) was used to measure MCD spectra. Magnetic properties were recorded on a Quantum Design MPMS-XL5 (SQUID) magnetometer (Quantum Design, San Diego, CA, USA). The diamagnetism of the molecule was corrected with Pascal's constant.

3.2. Nonlinear Optical (NLO) Response Measurements

An ultrafast fiber laser (NPI Lasers, Rainbow 1550 OEM) (PL OPTICS, Nanjing, China) was utilized as the excitation source to output 100 fs pulses at 1550 nm with a repetition rate of 80 MHz. This laser beam was then focused by an aspheric lens with a numerical aperture of 0.8, forming a laser spot with a beam waist radius of 2 μm . The spectra of the second-harmonic generation (SHG) and the third-harmonic generation (THG) were obtained using a cooled fiber optic spectrometer (Ideaoptics, NOVA, Shanghai, China). For comparison, the same integration time ($T_{\text{int}} = 0.5$ s) was used to obtain SHG and THG signals for the sample and reference material. The SHG and THG mappings were monitored by integrating SHG and THG spectra at different locations over an integration range of 500–550 nm and 750–800 nm for THG and SHG, respectively.

3.3. Synthesis of $\text{H}_2\text{L}_{\text{Schiff}}$

1-Hydroxy-2-naphthaldehyde (10 mmol) and pyrazinoic acid hydrazide (10 mmol) were added to 30 mL of methanol; the reaction mixture was refluxed for 3 h and then cooled to room temperature. The resulting light-yellow precipitate was collected by filtration and washed with 3×10 mL of ethanol before being dried in air. The yield was about 90%. The analytical calculations for $\text{H}_2\text{L}_{\text{Schiff}}$ ($\text{C}_{16}\text{H}_{12}\text{N}_4\text{O}_2$, %) are as follows: C, 65.75; H, 4.14; N, 19.17%; found (%): C, 65.56; H, 4.18; N, 19.07%. The FT-IR peaks (KBr, cm^{-1}) for $\text{H}_2\text{L}_{\text{Schiff}}$

are as follows: 3315 (m), 3052 (w), 1690 (s), 1635 (w), 1600 (m), 1565 (w), 1523 (m), 1502 (w), 1463 (w), 1402 (w), 1358 (w), 1315 (m), 1265 (w), 1227 (w), 1160 (m), 1146 (w), 1109 (w), 1095 (w), 1019 (m), 988 (w), 958 (w), 903 (w), 877 (w), 849 (w), 810 (m), 786 (w), 763 (w), 746 (w), 678 (w), 555 (m), 480 (w), 444 (w), and 427 (w).

3.4. Syntheses of L-1 and D-1

A mixture of H_2L_{Schiff} (0.25 mmol), *L/D*-proline (0.25 mmol), $Dy(CF_3SO_3)_3$ (0.25 mmol), and $LiOH \cdot H_2O$ (0.75 mmol) in 5 mL of DMA was stirred for 24 h to form a brownish-red solution, which was filtered and transferred to a beaker. By slowly evaporating the solvent, single red crystals of *L-1* and *D-1* appeared a few weeks later. The yield was as follows: about 20% based on Dy. The analytical calculations for *L-1* ($C_{147}H_{153}Dy_6N_{35}O_{34}$, %) are as follows: C, 44.94; H, 3.93; N, 12.48%; found (%): C, 44.89; H, 3.97; N, 12.45%. The FT-IR peaks (KBr, cm^{-1}) for *L-1* are as follows: 3434 (s, br), 3044 (w), 2935 (w), 2874 (w), 1595 (s), 1555 (m), 1534 (m), 1516 (w), 1497 (w), 1472 (m), 1433 (m), 1405 (m), 1327 (m), 1239 (w), 1201 (w), 1176 (w), 1151 (w), 1102 (w), 1056 (w), 1033 (w), 980 (w), 926 (w), 889 (w), 860 (w), 794 (w), 770 (w), 747 (w), 704 (w), 688 (w), 619 (w), 583 (w), 566 (w), 509 (w), 476 (w), and 429 (w). The analytical calculations for *D-1* ($C_{147}H_{153}Dy_6N_{35}O_{34}$, %) are as follows: C, 44.94; H, 3.93; N, 12.48%; found (%): C, 44.98; H, 3.97; N, 12.44%. The FT-IR peaks (KBr, cm^{-1}) for *D-1* are as follows: 3434 (s, br), 3044 (w), 2938 (w), 2875 (w), 1594 (s), 1555 (m), 1534 (m), 1516 (w), 1497 (w), 1472 (m), 1433 (m), 1406 (m), 1327 (m), 1238 (w), 1201 (w), 1176 (w), 1151 (w), 1102 (w), 1056 (w), 1034 (w), 980 (w), 926 (w), 889 (w), 860 (w), 794 (w), 771 (w), 748 (w), 704 (w), 688 (w), 619 (w), 583 (w), 566 (w), 509 (w), 476 (w), and 429 (w).

3.5. X-ray Single-Crystal Structure Measurement

Single-crystal diffraction data for *L-1* and *D-1* were collected on a Rigaku MM007HF (RIGAKU, Tokyo, Japan) diffractometer () with graphite-monochromated Mo-K α radiation ($\lambda = 0.71073 \text{ \AA}$) at 173 K. The two structures were solved using the olex2.solve structure solution program and refined using the ShelXL-2015 refinement package. The squeeze technology was adopted to refine these two structures since the lattice solvent molecules DMA and H_2O in *L-1* and *D-1* were disordered. Notably, the pyrrolidine ring in *L/D*-proline ligands was disordered in two positions and idealized by bond distances. All non-hydrogen atoms were refined anisotropically, and all hydrogen atoms were allowed for as riding atoms. The crystallographic data and refinement parameters are listed in Table 1.

Table 1. Crystal data and structural refinement parameters for *L-1* and *D-1*.

	<i>L-1</i> (Squeeze)	<i>D-1</i> (Squeeze)
formula	$C_{127}H_{104}Dy_6N_{30}O_{27}$	$C_{127}H_{104}Dy_6N_{30}O_{27}$
F_W	3457.40	3457.40
crystal system	monoclinic	monoclinic
space group	C2	C2
a [\AA]	33.8797(5)	33.8283(9)
b [\AA]	17.3214(2)	17.3710(4)
c [\AA]	26.3394(3)	26.3514(6)
β [$^\circ$]	102.5770(10)	102.613(2)
V [\AA^3]	15,086.2(3)	15,111.2(6)
Z	4	4
ρ_{calc} [$g \cdot cm^{-3}$]	1.522	1.520
μ [mm^{-1}]	3.006	3.002
T [K]	170	170

Table 1. Cont.

λ [Å]	0.71073	0.71073
reflections collected	142,419	132,511
unique reflections	41,244	39,636
observed reflections	33,159	29,637
parameters	1987	1981
GoF [$I \geq 2\sigma(I)$]	1.048	1.063
R_1 [$I \geq 2\sigma(I)$]	0.0568	0.0602
wR_2 [$I \geq 2\sigma(I)$]	0.1380	0.1439
Flack parameter	0.086(12)	0.005(7)
CCDC number	2,363,753	2,363,754

4. Conclusions

In summary, a pair of enantiomers with the novel triangular Dy₆ core was prepared using the new hydrazone Schiff base bridging ligand (E)-N'-((1-hydroxynaphthalen-2-yl)methylene)pyrazine-2-carbohydrazide and the chiral ligand L/D-proline. During the reaction, CO₂ in the air was fixed to form the carbonato ligand, which plays a critical role in the construction of the homochiral Dy₆ complexes as a central bridging ligand. This pair of homochiral Dy₆ clusters exhibited intramolecular ferromagnetic coupling and a frequency-dependent AC magnetic susceptibility and displayed a distinct magneto-optical Faraday effect and an SHG response as strong as KDP. This study demonstrates that the fixation of CO₂ in the air can be used to construct chiral cluster complexes, which provides a unique synthetic pathway for multifunctional molecular materials.

Supplementary Materials: The following supporting information can be downloaded at <https://www.mdpi.com/article/10.3390/molecules29143402/s1>: X-ray crystallographic data file in CIF format, CCDC number 2,363,753 for L-1 and 2,363,754 for D-1; Tables S1 and S2: Dy(III) ion geometry analysis for L-1 using SHAPE 2.1 software; Figure S1: M vs. H/T plots of L-1 at 2–6 K; Figure S2: plots of χ'' vs. T for L-1 at 1399 Hz ($H_{dc} = 0$ Oe and 2000 Oe); Figure S3: Debye plots of L-1 for the indicated AC frequencies; Figure S4: UV-vis spectra of H₂L_{Schiff} in DMF solution; Figure S5: MCD spectra of L-1 and D-1; Figure S6: g_{MCD} of L-1 and D-1.

Author Contributions: Conceptualization, C.-M.L.; methodology, C.-M.L.; validation, C.-M.L.; investigation, C.-M.L., X.H. and X.-L.L.; writing—original draft preparation, C.-M.L.; writing—review and editing, C.-M.L.; project administration, C.-M.L.; funding acquisition, C.-M.L. All authors have read and agreed to the published version of the manuscript.

Funding: This research was funded by the National Natural Science Foundation of China (grant numbers 22271289 and 21871274).

Institutional Review Board Statement: Not applicable.

Informed Consent Statement: Not applicable.

Data Availability Statement: Data are contained within the article and Supplementary Materials.

Conflicts of Interest: The authors declare no conflicts of interest.

References

- English, N.J.; El-Hendawy, M.M.; Mooney, D.A.; MacElroy, J.M.D. Perspectives on atmospheric CO₂ fixation in inorganic and biomimetic structures. *Coord. Chem. Rev.* **2014**, *269*, 85–95. [CrossRef]
- Guo, Y.-N.; Chen, X.-H.; Xue, S.; Tang, J. Molecular Assembly and Magnetic Dynamics of Two Novel Dy₆ and Dy₈ Aggregates. *Inorg. Chem.* **2012**, *51*, 4035–4042. [CrossRef]
- Tang, X.-L.; Wang, W.-H.; Dou, W.; Jiang, J.; Liu, W.-S.; Qin, W.-W.; Zhang, G.-L.; Zhang, H.-R.; Yu, K.-B.; Zheng, L.-M. Olive-Shaped Chiral Supramolecules: Simultaneous Self-Assembly of Heptameric Lanthanum Clusters and Carbon Dioxide Fixation. *Angew. Chem. Int. Ed.* **2009**, *48*, 3499–3502. [CrossRef]

4. Tian, H.; Guo, Y.-N.; Zhao, L.; Tang, J.; Liu, Z. Hexanuclear Dysprosium(III) Compound Incorporating Vertex- and Edge-Sharing Dy₃ Triangles Exhibiting Single-Molecule-Magnet Behavior. *Inorg. Chem.* **2011**, *50*, 8688–8690. [[CrossRef](#)] [[PubMed](#)]
5. Gass, I.A.; Moubaraki, B.; Langley, S.K.; Battena, S.R.; Murray, K.S. A π - π 3D network of tetranuclear μ_2/μ_3 -carbonato Dy(III) bis-pyrazolylpyridine clusters showing single molecule magnetism features. *Chem. Commun.* **2012**, *48*, 2089–2091. [[CrossRef](#)] [[PubMed](#)]
6. Tian, H.; Zhao, L.; Guo, Y.-N.; Guo, Y.; Tang, J.; Liu, Z. Quadruple-CO₃²⁻ bridged octanuclear dysprosium(III) compound showing single-molecule magnet behavior. *Chem. Commun.* **2012**, *48*, 708–710. [[CrossRef](#)] [[PubMed](#)]
7. Langley, S.K.; Gass, I.A.; Moubaraki, B.; Murray, K.S. Magnetic Properties of Hexanuclear Lanthanide (III) Clusters Incorporating a Central μ_6 -Carbonate Ligand Derived from Atmospheric CO₂ Fixation. *Inorg. Chem.* **2012**, *51*, 3947–3949. [[CrossRef](#)] [[PubMed](#)]
8. Tian, H.; Wang, M.; Zhao, L.; Guo, Y.-N.; Guo, Y.; Tang, J.; Liu, Z. A Discrete Dysprosium Trigonal Prism Showing Single-Molecule Magnet Behaviour. *Chem. Eur. J.* **2012**, *18*, 442–445. [[CrossRef](#)] [[PubMed](#)]
9. Holmberg, R.J.; Kuo, C.-J.; Gabidullin, B.; Wang, C.-W.; Clérac, R.; Murugesu, M.; Lin, P.-H. A propeller-shaped μ_4 -carbonate hexanuclear dysprosium complex with a high energetic barrier to magnetisation relaxation. *Dalton Trans.* **2016**, *45*, 16769–16773. [[CrossRef](#)] [[PubMed](#)]
10. Wang, W.-M.; Wu, Z.-L.; Zhang, Y.-X.; Wei, H.-Y.; Gao, H.-L.; Cui, J.-Z. Self-assembly of tetra-nuclear lanthanide clusters *via* atmospheric CO₂ fixation: Interesting solvent-induced structures and magnetic relaxation conversions. *Inorg. Chem. Front.* **2018**, *5*, 2346–2354. [[CrossRef](#)]
11. Kumar, P.; Swain, A.; Acharya, J.; Li, Y.; Kumar, V.; Rajaraman, G.; Colacio, E.; Chandrasekhar, V. Synthesis, Structure, and Zero-Field SMM Behavior of Homometallic Dy₂, Dy₄, and Dy₆ Complexes. *Inorg. Chem.* **2022**, *61*, 11600–11621. [[CrossRef](#)] [[PubMed](#)]
12. Liu, C.M.; Hao, X. Anion-dependent dysprosium(III) cluster single-molecule magnets. *New J. Chem.* **2023**, *47*, 18849–18855. [[CrossRef](#)]
13. Qin, L.; Zhou, G.-J.; Yu, Y.-Z.; Nojiri, H.; Schröder, C.; Winpenny, R.E.P.; Zheng, Y.-Z. Topological Self-Assembly of Highly Symmetric Lanthanide Clusters: A Magnetic Study of Exchange-Coupling “Fingerprints” in Giant Gadolinium(III) Cages. *J. Am. Chem. Soc.* **2017**, *139*, 16405–16411. [[CrossRef](#)] [[PubMed](#)]
14. Kitajima, N.; Fujisawa, K.; Koda, T.; Hikichi, S.; Moro-oka, Y. Fixation of atmospheric CO₂ by a copper(II) complex. *J. Chem. Soc. Chem. Commun.* **1990**, *19*, 1357–1358. [[CrossRef](#)]
15. Tanase, T.; Nitta, S.; Yoshikawa, S.; Kobayashi, K.; Sakurai, T.; Yano, S. Spontaneous fixation of carbon dioxide in air by a nickel diamine complex: Synthesis and characterization of a trinuclear nickel(II) complex with a novel hydrogen bonding system around a carbonate ligand. *Inorg. Chem.* **1992**, *31*, 1058–1062. [[CrossRef](#)]
16. El-Hendawy, M.M.; English, N.J.; Mooney, D.A. Mechanism of Atmospheric CO₂ Fixation in the Cavities of a Dinuclear Cryptate. *Inorg. Chem.* **2012**, *51*, 5282–5288. [[CrossRef](#)] [[PubMed](#)]
17. Wang, W.; Wen, Y.; Su, J.; Ma, H.; Wang, H.-Y.; Kurmoo, M.; Zuo, J.-L. Carbon Dioxide (CO₂) Fixation: Linearly Bridged Zn₂ Paddlewheel Nodes by CO₂ in a Metal-Organic Framework. *Inorg. Chem.* **2019**, *58*, 16040–16046. [[CrossRef](#)]
18. Tian, X.-F.; Ji, B.-Q.; Feng, L.; Sheng, K.; Su, Y.-M.; Jagodič, M.; Jagličič, Z.; Tung, C.-H.; Sun, D. Self-assembly of a nonanuclear Ni^{II} cluster *via* atmospheric CO₂ fixation: Synthesis, structure, collision-induced dissociation mass spectrometry and magnetic property. *Dalton Trans.* **2020**, *49*, 10977–10982. [[CrossRef](#)] [[PubMed](#)]
19. Sheng, K.; Wang, R.; Tang, X.; Jagodič, M.; Jagličič, Z.; Pang, L.; Dou, J.-M.; Gao, Z.-Y.; Feng, H.-Y.; Tung, C.-H.; et al. Carbonate-Templated Decanuclear Mn Nanocage with Two Different Silsesquioxane Ligands. *Inorg. Chem.* **2021**, *60*, 14866–14871. [[CrossRef](#)] [[PubMed](#)]
20. Kong, X.-J.; Ren, Y.-P.; Long, L.-S.; Zheng, Z.; Huang, R.-B.; Zheng, L.-S. A Keplerate Magnetic Cluster Featuring an Icosidodecahedron of Ni(II) Ions Encapsulating a Dodecahedron of La(III) Ions. *J. Am. Chem. Soc.* **2007**, *129*, 701–7017. [[CrossRef](#)] [[PubMed](#)]
21. Titos-Padilla, S.; Ruiz, J.; Herrera, J.M.; Brechin, E.K.; Wersndorfer, W.; Lloret, F.; Colacio, E. Dilution-Triggered SMM Behavior under Zero Field in a Luminescent Zn₂Dy₂ Tetranuclear Complex Incorporating Carbonato-Bridging Ligands Derived from Atmospheric CO₂ Fixation. *Inorg. Chem.* **2013**, *52*, 9620–9626. [[CrossRef](#)] [[PubMed](#)]
22. Sakamoto, S.; Fujinami, K.; Nishi, N.; Matsumoto, N.; Mochida, T.; Ishida, Y.; Sunatsuki, N.; Re, N. Carbonato-Bridged Ni^{II}₂Ln^{III}₂ (Ln^{III} = Gd^{III}, Tb^{III}, Dy^{III}) Complexes Generated by Atmospheric CO₂ Fixation and Their Single-Molecule-Magnet Behavior: [(μ_4 -CO₃)₂{Ni^{II}(3-MeOsalt)(MeOH or H₂O)Ln^{III}(NO₃)₂}]·solvent [3-MeOsalt = N,N'-Bis(3-methoxy-2-oxybenzylidene)-1,3-propanediaminato]. *Inorg. Chem.* **2013**, *52*, 7218–7229. [[PubMed](#)]
23. Zhang, P.; Zhang, L.; Lin, S.-Y.; Tang, J. Tetranuclear [MDy]₂ Compounds and Their Dinuclear [MDy] (M = Zn/Cu) Building Units: Their Assembly, Structures, and Magnetic Properties. *Inorg. Chem.* **2013**, *52*, 6595–6602. [[CrossRef](#)] [[PubMed](#)]
24. Ruiz, J.; Lorusso, G.; Evangelisti, M.; Brechin, E.K.; Pope, S.J.A.; Colacio, E. Closely-Related Zn^{II}₂Ln^{III}₂ Complexes (Ln^{III} = Gd, Yb) with Either Magnetic Refrigerant or Luminescent Single-Molecule Magnet Properties. *Inorg. Chem.* **2014**, *53*, 3586–3594. [[CrossRef](#)]
25. Upadhyay, A.; Das, C.; Langley, S.K.; Murray, K.S.; Srivastava, A.K.; Shanmugam, M. Heteronuclear Ni(ii)-Ln(iii) (Ln = La, Pr, Tb, Dy) complexes: Synthesis and single-molecule magnet behavior. *Dalton Trans.* **2016**, *45*, 3616–3626. [[CrossRef](#)] [[PubMed](#)]

26. Wen, H.-R.; Hu, J.-J.; Yang, K.; Zhang, J.-L.; Liu, S.-J.; Liao, J.-S.; Liu, C.-M. Family of Chiral Zn^{II}-Ln^{III} (Ln = Dy and Tb) Heterometallic Complexes Derived from the Amine-Phenol Ligand Showing Multifunctional Properties. *Inorg. Chem.* **2020**, *59*, 2811–2824. [[CrossRef](#)]
27. Liu, C.-M.; Zhang, D.-Q.; Hao, X.; Zhu, D.-B. Zn₂Ln₂ complexes with carbonate bridges formed by the fixation of carbon dioxide in the atmosphere: Single-molecule magnet behaviour and magnetocaloric effect. *Dalton Trans.* **2020**, *49*, 2121–2128. [[CrossRef](#)] [[PubMed](#)]
28. Liu, C.-M.; Hao, X.; Zhang, D.-Q. Effects of substituents on bridging ligands on the single-molecule magnet properties of Zn₂Dy₂ cluster complexes. *Appl. Organometal. Chem.* **2021**, *35*, e6048. [[CrossRef](#)]
29. Sheikh, J.A.; Jena, H.S.; Konar, S. Co₃Gd₄ Cage as Magnetic Refrigerant and Co₃Dy₃ Cage Showing Slow Relaxation of Magnetisation. *Molecules* **2022**, *27*, 1130. [[CrossRef](#)] [[PubMed](#)]
30. Gatteschi, D.; Sessoli, R. Quantum Tunneling of Magnetization and Related Phenomena in Molecular Materials. *Angew. Chem. Int. Ed.* **2003**, *42*, 268–297. [[CrossRef](#)]
31. Leuenberger, M.N.; Loss, D. Quantum computing in molecular magnets. *Nature* **2001**, *410*, 789–793. [[CrossRef](#)]
32. Woodruff, D.N.; Winpenny, R.E.P.; Layfield, R.A. Lanthanide Single-Molecule Magnets. *Chem. Rev.* **2013**, *113*, 5110–5148. [[CrossRef](#)]
33. Goodwin, C.A.P.; Ortu, F.; Reta, D.; Chilton, N.F.; Mills, D.P. Molecular magnetic hysteresis at 60 kelvin in dysprosocenium. *Nature* **2017**, *548*, 439–442. [[CrossRef](#)] [[PubMed](#)]
34. Guo, F.S.; Day, B.M.; Chen, Y.C.; Tong, M.L. Magnetic hysteresis up to 80 kelvin in a dysprosium metallocene single-molecule magnet. *Science* **2018**, *362*, 1400–1403. [[CrossRef](#)] [[PubMed](#)]
35. Liu, J.; Chen, Y.C.; Liu, J.L.; Vieru, V.; Ungur, L.; Jia, J.H.; Chibotaru, L.F.; Lan, Y.H.; Wernsdorfer, W.; Gao, S.; et al. A Stable Pentagonal-Bipyramidal Dy(III) Single-Ion Magnet with a Record Magnetization Reversal Barrier over 1000 K. *J. Am. Chem. Soc.* **2016**, *138*, 5441–5450. [[CrossRef](#)] [[PubMed](#)]
36. Meng, Y.S.; Jiang, S.D.; Wang, B.W.; Gao, S. Understanding the Magnetic Anisotropy toward Single-Ion Magnets. *Acc. Chem. Res.* **2016**, *49*, 2381–2389. [[CrossRef](#)] [[PubMed](#)]
37. Ding, Y.S.; Chilton, N.F.; Winpenny, R.E.; Zheng, Y.Z. On Approaching the Limit of Molecular Magnetic Anisotropy: A Near-Perfect Pentagonal Bipyramidal Dysprosium(III) Single-Molecule Magnet. *Angew. Chem. Int. Ed.* **2016**, *55*, 16071–16074. [[CrossRef](#)] [[PubMed](#)]
38. Liu, C.M.; Zhang, D.Q.; Hao, X.; Zhu, D.B. Assembly of chiral 3d-4f wheel-like cluster complexes with achiral ligands: Single-molecule magnetic behavior and magnetocaloric effect. *Inorg. Chem. Front.* **2020**, *7*, 3340–3351. [[CrossRef](#)]
39. Liu, C.M.; Zhu, S.D.; Lu, Y.B.; Hao, X.; Wen, H.R. Homochiral Cu₆Dy₃ single-molecule magnets displaying proton conduction and a strong magneto-optical Faraday effect. *Inorg. Chem. Front.* **2023**, *10*, 3714–3722. [[CrossRef](#)]
40. Liu, C.M.; Sun, R.; Wang, B.W.; Wu, F.; Hao, X.; Shen, Z. Homochiral Ferromagnetic Coupling Dy₂ Single-Molecule Magnets with Strong Magneto-Optical Faraday Effects at Room Temperature. *Inorg. Chem.* **2021**, *60*, 12039–12048. [[CrossRef](#)] [[PubMed](#)]
41. Liu, C.M.; Sun, R.; Hao, X.; Wang, B.-W. Two Pairs of Homochiral Parallelogram-like Dy₄ Cluster Complexes with Strong Magneto-Optical Properties. *Inorg. Chem.* **2023**, *62*, 20184–20193. [[CrossRef](#)] [[PubMed](#)]
42. Liu, C.M.; Sun, R.; Hao, X.; Li, X.-L.; Wang, B.-W. Homochiral Dy₂ single-molecule magnets with strong magneto-optical Faraday effects and strong third-harmonic generation. *Inorg. Chem. Front.* **2024**, *11*, 3296–3308. [[CrossRef](#)]
43. Wang, K.; Zeng, S.; Wang, H.; Dou, J.; Jiang, J. Magneto-chiral dichroism in chiral mixed (phthalocyaninato)(porphyrinato) rare earth triple-decker SMMs. *Inorg. Chem. Front.* **2014**, *1*, 167–171. [[CrossRef](#)]
44. Wang, X.; Du, M.-H.; Xu, H.; Long, L.-S.; Kong, X.-J.; Zheng, L.-S. Cocrystallization of Chiral 3d-4f Clusters {Mn₁₀Ln₆} and {Mn₆Ln₂}. *Inorg. Chem.* **2021**, *60*, 5925–5930. [[CrossRef](#)] [[PubMed](#)]
45. Zhu, S.-D.; Zhou, Y.-L.; Liu, F.; Lei, Y.; Liu, S.-J.; Wen, H.-R.; Shi, B.; Zhang, S.-Y.; Liu, C.-M.; Lu, Y.-B. A Pair of Multifunctional Cu(II)-Dy(III) Enantiomers with Zero-Field Single-Molecule Magnet Behaviors, Proton Conduction Properties and Magneto-Optical Faraday Effects. *Molecules* **2023**, *28*, 7506. [[CrossRef](#)] [[PubMed](#)]
46. Huang, H.; Sun, R.; Wu, X.-F.; Liu, Y.; Zhan, J.-Z.; Wang, B.-W.; Gao, S. Circularly polarized luminescence and magneto-optic effects from chiral Dy(III) single molecule magnets. *Dalton Trans.* **2023**, *52*, 7646–7651. [[CrossRef](#)] [[PubMed](#)]
47. Dhbaibi, K.; Grasser, M.; Douib, H.; Dorcet, V.; Cador, O.; Vanthuyne, N.; Riobé, F.; Maury, O.; Guy, S.; Bensalah-Ledoux, A.; et al. Multifunctional Helicene-Based Ytterbium Coordination Polymer Displaying Circularly Polarized Luminescence, Slow Magnetic Relaxation and Room Temperature Magneto-Chiral Dichroism. *Angew. Chem. Int. Ed.* **2023**, *62*, e202215558. [[CrossRef](#)] [[PubMed](#)]
48. Liu, C.-M.; Xiong, R.-G.; Zhang, D.-Q.; Zhu, D.-B. Nanoscale Homochiral C₃-Symmetric Mixed-Valence Manganese Cluster Complexes with Both Ferromagnetic and Ferroelectric Properties. *J. Am. Chem. Soc.* **2010**, *132*, 4044–4045. [[CrossRef](#)] [[PubMed](#)]
49. Thielemann, D.T.; Wagner, A.T.; Lan, Y.; Anson, C.E.; Gamer, M.T.; Powell, A.K.; Roesky, P.W. Slow magnetic relaxation in four square-based pyramidal dysprosium hydroxo clusters ligated by chiral amino acid anions—a comparative study. *Dalton Trans.* **2013**, *42*, 14794–14800. [[CrossRef](#)] [[PubMed](#)]
50. Casanova, D.; Lluell, M.; Alemany, P.; Alvarez, S. The Rich Stereochemistry of Eight-Vertex Polyhedra: A Continuous Shape Measures Study. *Chem.-Eur. J.* **2005**, *11*, 1479–1494. [[CrossRef](#)] [[PubMed](#)]
51. Liu, C.-M.; Hao, X.; Zhu, D.-M.; Zhang, Y.-Q. Effect of coordinated anions on ferromagnetically coupled Dy₂ zero-field single-molecule magnets. *Dalton Trans.* **2024**, *53*, 6120–6127. [[CrossRef](#)] [[PubMed](#)]

52. Bartolomé, J.; Filoti, G.; Kuncser, V.; Schinteie, G.; Mereacre, V.; Anson, C.E.; Powell, A.K.; Prodius, D.; Turta, C. Magnetostructural correlations in the tetranuclear series of $\{\text{Fe}_3\text{LnO}_2\}$ butterfly core clusters: Magnetic and Mössbauer spectroscopic study. *Phys. Rev. B* **2009**, *80*, 014430–014446. [[CrossRef](#)]
53. Pantelis, K.N.; Perlepe, P.S.; Grammatikopoulos, S.; Lampropoulos, C.; Tang, J.; Stamatatos, T.C. 4f-Metal Clusters Exhibiting Slow Relaxation of Magnetization: A $\{\text{Dy}_7\}$ Complex with An Hourglass-like Metal Topology. *Molecules* **2020**, *25*, 2191. [[CrossRef](#)] [[PubMed](#)]
54. Bhattacharya, P.; Bag, R.; Satpathi, S.; Pati, S.K.; Butcher, R.J.; Tang, J.; Goswami, S. Structure and Magnetism of Ln^{III}_2 (Ln = Gd, Tb, Dy, and Ho) Assemblies Constructed from a Bis(Hydrazone) Compartmental Ligand: Slow Magnetic Relaxation in the Dy^{III}_2 Analogue. *Cryst. Growth Des.* **2023**, *23*, 7459–7471. [[CrossRef](#)]
55. Ewing, G.W.; Steck, E.A. Absorption spectra of heterocyclic compounds. I. Quinolinols and isoquinolinols. *J. Am. Chem. Soc.* **1946**, *68*, 2181–2187. [[CrossRef](#)] [[PubMed](#)]
56. Rikken, G.L.J.A.; Raupach, E. Enantioselective magnetochiral photochemistry. *Nature* **2000**, *405*, 932–935. [[CrossRef](#)] [[PubMed](#)]
57. Liu, C.M.; Sun, R.; Wang, B.-W.; Hao, X.; Li, X.-L. Effects of Counterions, Coordination Anions, and Coordination Solvent Molecules on Single-Molecule Magnetic Behaviors and Nonlinear Optical Properties of Chiral Zn_2Dy Schiff Base Complexes. *Inorg. Chem.* **2022**, *61*, 18510–18523. [[CrossRef](#)] [[PubMed](#)]
58. Li, X.-L.; Wang, A.; Cui, M.; Gao, C.; Yu, X.; Su, B.; Zhou, L.; Liu, C.-M.; Xiao, H.-P.; Zhang, Y.-Q. Modulating Two Pairs of Chiral Dy^{III} Enantiomers by Distinct β -Diketone Ligands to Show Giant Differences in Single-Ion Magnet Performance and Nonlinear Optical Response. *Inorg. Chem.* **2022**, *61*, 9283–9294. [[CrossRef](#)] [[PubMed](#)]
59. Liu, C.-M.; Zhang, D.-Q.; Xiong, R.-G.; Hao, X.; Zhu, D.-B. A homochiral Zn-Dy heterometallic left-handed helical chain complex without chiral ligands: Anion-induced assembly and multifunctional integration. *Chem. Commun.* **2018**, *54*, 13379–13382. [[CrossRef](#)] [[PubMed](#)]
60. Zhu, S.-D.; Hu, J.-J.; Dong, L.; Wen, H.-R.; Liu, S.-J.; Lu, Y.-B.; Liu, C.-M. Multifunctional Zn(II)-Yb(III) complex enantiomers showing second-harmonic generation, near-infrared luminescence, single-molecule magnet behaviour and proton conduction. *J. Mater. Chem. C* **2020**, *8*, 16032–16041. [[CrossRef](#)]

Disclaimer/Publisher’s Note: The statements, opinions and data contained in all publications are solely those of the individual author(s) and contributor(s) and not of MDPI and/or the editor(s). MDPI and/or the editor(s) disclaim responsibility for any injury to people or property resulting from any ideas, methods, instructions or products referred to in the content.